

Dimuon production associated with a scalar intermediate boson carrying dileptonic quantum number*

Stephen L. Adler, J. B. Healy, Inga Karliner, Judy Lieberman, Yee Jack Ng, and Hung-Sheng Tsao

The Institute for Advanced Study, Princeton, New Jersey 08540

(Received 2 July 1975)

We calculate the production cross section and kinematic distributions for dimuons arising from the production of a heavy scalar intermediate boson carrying dileptonic quantum number. The low hadron recoil energy and low effective recoiling invariant masses found in this process exclude it as a candidate for the dimuon events recently observed in experiments at the Fermi National Accelerator Laboratory.

The recent observation of energetic dimuon events¹ in neutrino experiments at the Fermi National Accelerator Laboratory (Fermilab) has prompted the examination of various theoretical mechanisms for dimuon production. Among those considered to date are the existence of a new hadronic quantum number ("charm" or its variants),² production of a heavy neutral lepton,³ and production of a weak vector intermediate boson.⁴ We consider in this note a variant on the intermediate boson production model, in which the produced boson is a scalar particle carrying dileptonic quantum number.⁵ Such particles arise if one attempts⁶ to build a renormalizable field-theory model for weak interactions based on the *Fierz transform* of the usual $V-A$ leptonic effective Lagrangian,

$$\mathcal{L}_{\text{eff}}^{\text{muon}} = \frac{G}{\sqrt{2}} \bar{\nu}_\mu \gamma_\lambda (1 - \gamma_5) \mu \bar{\mu} \gamma^\lambda (1 - \gamma_5) \nu_\mu \quad (1a)$$

$$\stackrel{\text{Fierz transform}}{=} \sqrt{2} G \bar{\mu} (1 + \gamma_5) \nu_\mu^c \bar{\nu}_\mu^c (1 - \gamma_5) \nu_\mu, \quad (1b)$$

with c denoting charge-conjugate spinors. Evidently, if one postulates a scalar dileptonic intermediate boson B with the coupling to muons

$$\mathcal{L} = g \bar{\mu}^c (1 - \gamma_5) \nu_\mu B + \text{adjoint}, \quad (2)$$

$$g = 2^{1/4} M_B G^{1/2},$$

Equation (1b) is obtained in the tree approximation in the limit of large M_B . More generally, one can consider B production independent of the requirement that it account for the usual current-current leptonic Lagrangian, in which case the coupling constant g becomes a parameter to be fixed by experiment. In this generalized version, kinematic characteristics of the dimuons resulting from B production and decay become the decisive test of the model.

Specifically, the process we consider is

$$\nu_\mu(k_1) + p(p_1) \rightarrow \mu^+(k_2) + p(p_2) + B^-(q) \rightarrow \nu_\mu(q_1) + \mu^-(q_2), \quad (3)$$

which arises from the two Feynman diagrams shown in Fig. 1. This reaction is actually only one of three which contribute to the B production cross section; the other two are inelastic production, with the final proton in Eq. (3) replaced by a general baryonic final state, and (for nuclear targets) coherent production from the entire target nucleus. However, in their detailed studies of these three production mechanisms in the context of ordinary vector intermediate boson production, Brown and Smith⁴ found the analog of Eq. (3) to be the single most important contribution at Fermilab energies, accounting for about half of the total production cross section. Since the dileptonic boson production process being studied here is kinematically similar to vector-boson production, it seems reasonable to focus on the process of Eq. (3) in seeking a first estimate of the resulting dimuon production characteristics.

Using standard trace techniques, we have evaluated the cross section for Eq. (3); the results are summarized in the Appendix, together with some changes of integration variable which facilitated the numerical integrations. Production cross sections for a range of neutrino energies

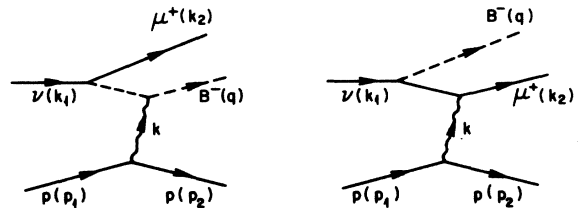


FIG. 1. Feynman diagrams for B production. The wavy line denotes a virtual photon.

E and boson masses M_B are given in Table I, corresponding to the choice of the coupling g given in Eq. (2). For $M_B \sim 5$ GeV, we find a cross section ratio $\sigma(E=150 \text{ GeV})/\sigma(E=50 \text{ GeV}) \approx 10$, consistent with observations in the Caltech-Fermilab dichromatic neutrino beam.¹ For this value of the boson mass, a reduction of the coupling g by roughly a factor of 5 from the value specified in Eq. (2) is necessary to bring the cross-section magnitudes down to the range⁷ observed for dimuon production at Fermilab. The calculation of histograms for dimuon production characteristics is greatly facilitated by the fact that decay of the scalar B particle is isotropic in its rest frame. A sampling of the histograms which we have computed for $M_B = 5$ GeV is given in Figs. 2 and 3. In Fig. 2 we have assumed a monoenergetic 150-GeV incident neutrino beam, corresponding to the higher energy component of the Caltech-Fermilab dichromatic beam, while in Fig. 3 we have assumed a neutrino-antineutrino mixture corresponding to the 380-GeV quadrupole triplet beam used in recent running of Fermilab experiment 1A.⁸ From the histograms, we

TABLE I. B production cross sections.

E (GeV)	Cross sections (10^{-38} cm^2)		
	$M_B = 2 \text{ GeV}$	$M_B = 5 \text{ GeV}$	$M_B = 8 \text{ GeV}$
20	12.6	0.4×10^{-4}	...
40	33.7	1.1	...
50	43.0	2.7	0.7×10^{-3}
70	58.9	7.4	0.16
90	72.1	12.9	0.89
110	83.6	18.6	2.2
130	93.6	24.3	4.1
150	103	29.8	6.2
170	111	35.2	8.6
190	118	40.4	11.1
210	124	45.4	13.7
250	136	54.9	19.0
290	147	63.6	24.3

see that in a neutrino beam the mean μ^- energy is substantially higher than the mean μ^+ energy, even though the μ^+ is produced at the incident lepton vertex. The muon energy distributions, dilepton angle $\theta_{\mu\mu}$, and dilepton invariant mass

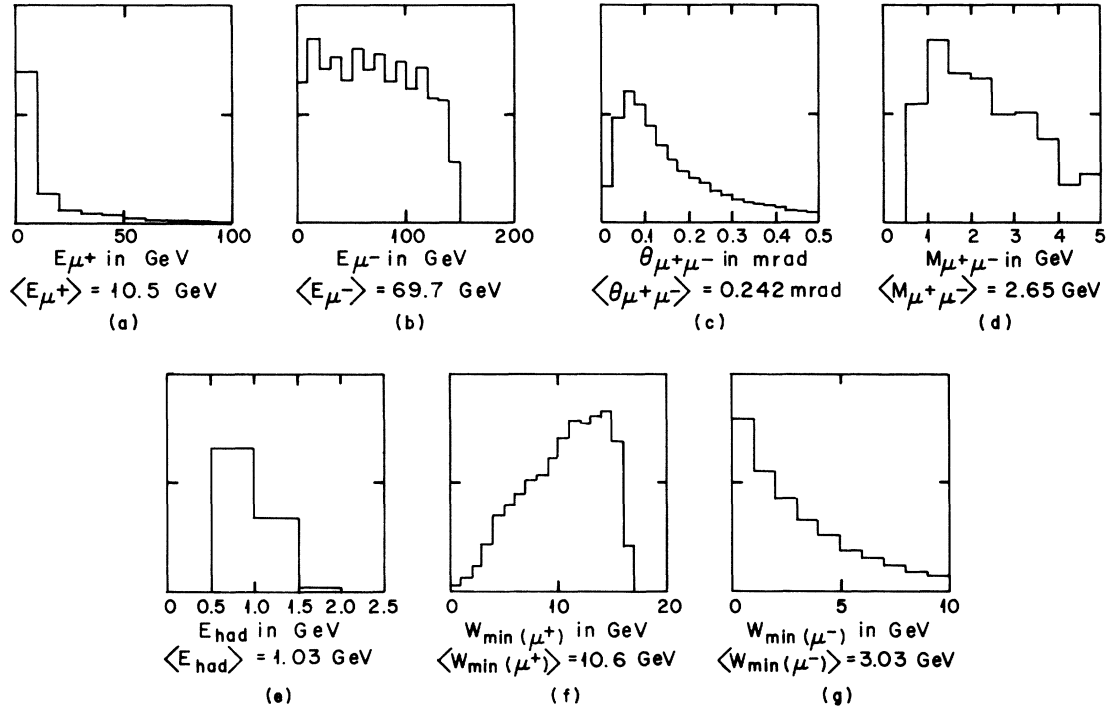


FIG. 2. Histograms calculated for a 150 GeV incident neutrino beam: (a) positive-muon laboratory energy E_{μ^+} , (b) negative-muon laboratory energy E_{μ^-} , (c) dimuon opening angle, (d) dimuon invariant mass, (e) recoil hadron laboratory energy $E_{\text{had}} = p_2^0$, (f) minimum effective invariant mass recoiling against the μ^+ , defined by $W_{\text{min}}(\mu^+)^2 = 2M_N(1 - V_{\mu^+})(E_{\text{had}} + E_{\mu^-}) + M_N^2 - 2M_N E_{\mu^+} V_{\mu^+}$, with $V_{\mu^+} = 2(E_{\mu^+}/M_N)\sin^2(\theta_{\mu^+}/2)$ and with θ_{μ^+} the laboratory angle between the μ^+ and the incident neutrino direction, (g) minimum effective invariant mass recoiling against the μ^- , defined by $W_{\text{min}}(\mu^-)^2 = 2M_N(1 - V_{\mu^-})(E_{\text{had}} + E_{\mu^+}) + M_N^2 - 2M_N E_{\mu^-} V_{\mu^-}$, with $V_{\mu^-} = 2(E_{\mu^-}/M_N)\sin^2(\theta_{\mu^-}/2)$ and with θ_{μ^-} the laboratory angle between the μ^- and the incident neutrino direction. The ordinate scales are arbitrary.

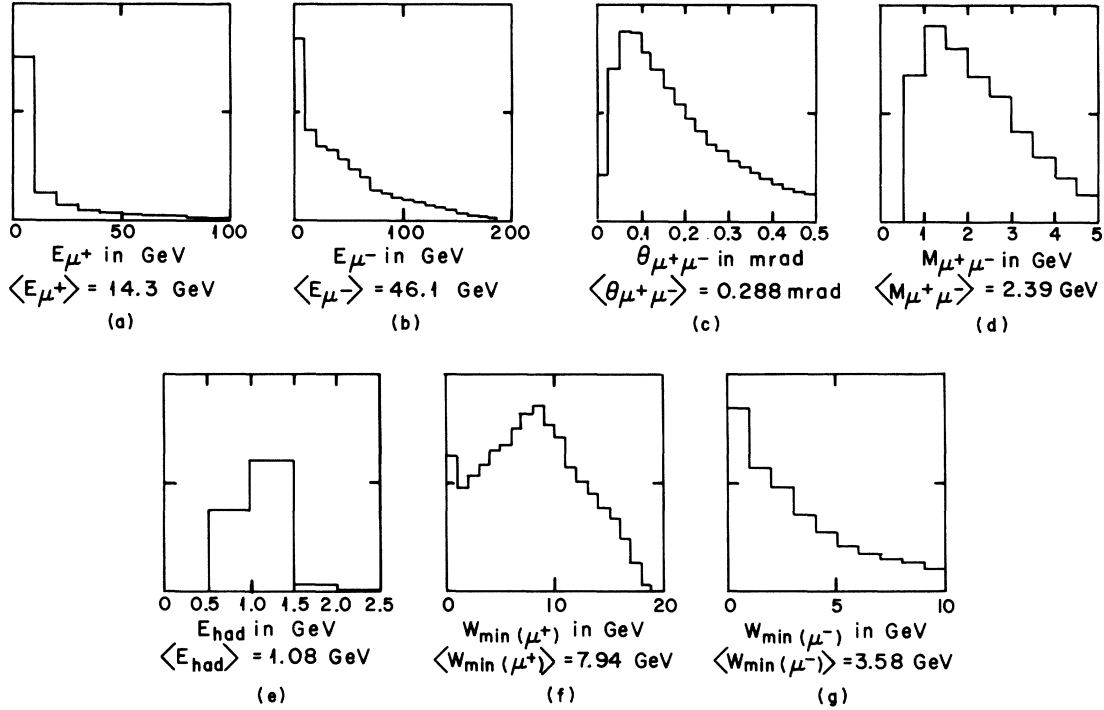


FIG. 3. Histograms for a neutrino-antineutrino mixture corresponding to 380 GeV primary protons with quadrupole triplet focusing: (a) positive-muon laboratory energy E_{μ^+} , (b) negative-muon laboratory energy E_{μ^-} , (c) dimuon opening angle, (d) dimuon invariant mass, (e) recoil hadron laboratory energy $E_{\text{had}} = p_{20}^L$, (f) minimum effective invariant mass recoiling against the μ^+ , (g) minimum effective invariant mass recoiling against the μ^- . The effective masses histogrammed in (f) and (g) are as defined in Fig. 2. The ordinate scales are arbitrary.

$M_{\mu\mu}$ are all in reasonable qualitative accord with the Fermilab dilepton observations. However, agreement is not good when we turn to the histogram for the recoil hadron energy and the minimum effective invariant recoil masses. The recoil hadron energy histogram shows a strong peaking at low energy, characteristic of that found in ordinary vector intermediate boson production.⁹ Experimentally, this would correspond to a small energy deposition in the hadron calorimeter ("quiet events"), whereas the observed Fermilab dimuons¹ are predominantly accompanied by large energy deposition in the calorimeter ("noisy events"). The calculated minimum effective invariant mass recoiling against the μ^- shows a peaking at small mass values, while the observed dimuons show essentially no events with this quantity less than 5 GeV. We conclude on the basis of these comparisons that the dileptonic boson process which we have examined is excluded¹⁰ as the principal production mechanism for the dimuon events observed at Fermilab.

We wish to thank A. K. Mann and T. Y. Ling for helpful conversations, and for supplying the

ν and $\bar{\nu}$ flux tables used in calculating the histograms of Fig. 3. One of us (S.L.A.) wishes to acknowledge the hospitality of the Fermilab theory group, where parts of this work were done.

APPENDIX

Fixing the coupling g as in Eq. (2), we find that the B -production cross section in the center-of-mass frame of the final B and μ^+ (the frame where $\vec{q} + \vec{k}_2 = \vec{0}$) is given by

$$\frac{d\sigma}{d\Omega_B} = \frac{\sqrt{2} GM_B^2 \alpha^2}{8\pi^2 M_N^2 E^2} \int_{x_{\min}}^{x_{\max}} \frac{dx}{x^2} \int_{y_{\min}}^{y_{\max}} dy \frac{|\vec{q}|}{W} \Sigma, \quad (\text{A1})$$

with α the fine-structure constant, G the Fermi constant, E the incident laboratory neutrino energy, and M_N and M_B respectively the nucleon and the scalar boson masses. Using the metric $(1, -1, -1, -1)$, the cross section Σ and the kinematic quantities needed in its evaluation are given as follows, with m_μ the muon mass:

$$x = -(\rho_1 - \rho_2)^2,$$

$$\left(\frac{x_{\max}}{x_{\min}} \right) = \frac{2E^2 - [(E + M_N)/M_N] (M_B + m_\mu)^2 \pm 2E \{ (E - E_T) [E - (M_B + m_\mu)^2 / 2M_N + M_B + m_\mu] \}^{1/2}}{1 + 2E/M_N},$$

$$E_T = \frac{(M_B + M_N + m_\mu)^2 - M_N^2}{2M_N}, \quad k = \rho_1 - \rho_2, \quad (\text{A2})$$

$$y = -k_1 \cdot k, \quad y_{\max} = -\frac{1}{2} [x + (M_B + m_\mu)^2], \quad y_{\min} = (E/2M_N) \{ x - [x(x + 4M_N^2)]^{1/2} \},$$

$$W = [(q + k_2)^2]^{1/2} = (-x - 2y)^{1/2}, \quad |\vec{q}| = (1/2W) \{ [W^2 - (M_B + m_\mu)^2] [W^2 - (M_B - m_\mu)^2] \}^{1/2},$$

$$\begin{aligned} \Sigma = & C_1 [3xW_1 - (4M_N^2 + x)W_2] + C_2 \{ [-xM_B^2 - (q \cdot k)^2] W_1 + (q \cdot P)^2 W_2 \} \\ & + C_3 \{ [-2xq \cdot k_2 - 2q \cdot k k \cdot k_2] W_1 + 2q \cdot P k_2 \cdot P W_2 \} + C_4 \{ [-m_\mu^2 x - (k \cdot k_2)^2] W_1 + (k_2 \cdot P)^2 W_2 \}, \end{aligned}$$

$$C_1 = \frac{1}{B^2} [xk_1 \cdot k_2 + 2k \cdot k_1 k \cdot k_2], \quad C_2 = -\frac{4k \cdot k_2}{AB} + \frac{4k_1 \cdot k_2}{A^2}, \quad (\text{A3})$$

$$C_3 = \frac{1}{B} - \frac{1}{AB} [4k_1 \cdot k_2 - 2k \cdot k_1 + 2k \cdot k_2], \quad C_4 = \frac{2}{B} - \frac{1}{B^2} [4k \cdot k_1 - 4k_1 \cdot k_2],$$

$$A = x + 2q \cdot k, \quad B = x + 2k \cdot k_2,$$

$$W_1 = W_1(x) = [F_1^p(x) + F_2^p(x)]^2, \quad W_2 = W_2(x) = F_1^p(x)^2 + xF_2^p(x)^2 / (4M_N^2).$$

In Eq. (A3), F_1^p and F_2^p are the usual proton electromagnetic form factors. Writing $d\Omega_B = \sin\phi d\phi d\delta$, the remaining kinematic quantities appearing in Eq. (A3) are given by

$$\begin{aligned} k \cdot k_1 &= k^0 |\vec{k}| + |\vec{k}|^2, \\ k \cdot k_2 &= k^0 k_2^0 - |\vec{k}| |\vec{q}| \cos\phi, \\ k \cdot q &= k^0 q^0 + |\vec{k}| |\vec{q}| \cos\phi, \\ k_1 \cdot k_2 &= k_2^0 |\vec{k}| + |\vec{k}| |\vec{q}| \cos\phi, \\ q \cdot k_2 &= k_2^0 q^0 + |\vec{q}|^2, \\ P &= \rho_1 + \rho_2, \\ k_2 \cdot P &= k_2^0 P^0 + P_x |\vec{q}| \sin\phi \cos\delta + P_z |\vec{q}| \cos\phi, \\ q \cdot P &= q^0 P^0 - P_x |\vec{q}| \sin\phi \cos\delta - P_z |\vec{q}| \cos\phi, \end{aligned} \quad (\text{A4})$$

with

$$\begin{aligned} k_2^0 &= (W^2 + m_\mu^2 - M_B^2) / (2W), \\ q^0 &= (W^2 + M_B^2 - m_\mu^2) / (2W), \\ k^0 &= (W^2 - x) / (2W), \\ P^0 &= (4EM_N - W^2 - x) / (2W), \\ |\vec{k}| &= (W^2 + x) / (2W), \\ P_z &= -(k^0 / |\vec{k}|) P^0, \\ P_x &= \{ (P^0)^2 [1 - (k^0 / |\vec{k}|)^2] - 4M_N^2 - x \}^{1/2}. \end{aligned} \quad (\text{A5})$$

In doing the numerical integrations, we found it expedient to make the following changes of variable:

$$\begin{aligned} \frac{dx}{x} &= dz, \quad \frac{dy}{(-y)^{1.75}} = dw; \\ \frac{d\cos\phi}{D - \cos\phi} &= ds \text{ for } 0.75 \leq \cos\phi \leq 1.0, \\ D &= (x + 2k^0 k_2^0) / 2 |\vec{q}| |\vec{k}|. \end{aligned} \quad (\text{A6})$$

The actual procedure employed in getting the cross section table was to do the δ and $\cos\phi$ integrations analytically,¹¹ with the result

$$\int d\Omega_B \frac{|\vec{q}|}{W} \Sigma = 2\pi\hat{\Sigma},$$

with

$$\begin{aligned} \hat{\Sigma} &= \hat{T}_2 \left\{ x W_1 + W_2 \left[-2M_N^2 + \frac{2M_N E x}{y^2} (M_N E + y) \right] \right\} + \hat{T}_1 W_2 \left[2M_N^2 - x - \frac{6M_N E x}{y^2} (M_N E + y) \right], \\ \hat{T}_1 &= -\frac{x}{y^3} \left[\left(y\Delta - \frac{\Delta^3}{2y} \right) I_2 + \frac{1}{2} \left(2y\Delta - y^2 - \frac{\Delta^3}{y} \right) I_3 + \frac{1}{2} \Delta(\Delta + 2y) I_4 + \frac{1}{2} (y - \Delta)^2 I_5 \right], \\ \hat{T}_2 &= \frac{1}{y} \left[\left(x + 2y + 2\Delta + \frac{M_B^4 - m_\mu^4}{y} \right) I_2 + \left(\frac{x}{2} + 2\Delta + \frac{M_B^4 - m_\mu^4}{y} \right) I_3 + (x - 2m_\mu^2) I_4 - \frac{1}{2} (x + 4M_B^2) I_5 \right], \\ I_2 &= -\frac{1}{2} \ln \left[\frac{y(x+2y) + \Delta(x+y) + yR}{y(x+2y) + \Delta(x+y) - yR} \right], \quad I_3 = -\frac{1}{2} \ln \left[\frac{y(x+2y) - \Delta(x+y) + yR}{y(x+2y) - \Delta(x+y) - yR} \right], \\ I_4 &= \frac{y\Delta R}{-4m_\mu^2 y^2 + 2xy\Delta + x\Delta^2}, \quad I_5 = \frac{y\Delta R}{-4M_B^2 y^2 - 2xy\Delta + x\Delta^2}, \\ \Delta &= M_B^2 - m_\mu^2, \quad R = [(-x - 2y - \Delta)^2 + 4m_\mu^2(x + 2y)]^{1/2}. \end{aligned} \tag{A7}$$

This left only the x and y integrations to be done numerically and permitted calculation of the cross sections to good accuracy using little computer time. Calculation of the histograms involved a sixfold numerical integration (over x , y , ϕ , δ , and two angles describing the B -particle decay); the integration meshes used reproduced the cross sections of Table I to within about one percent.

*Research sponsored in part by the U. S. Atomic Energy Commission, Grant No. AT(11-1)-2220.

¹A. Benvenuti *et al.*, Phys. Rev. Lett. **34**, 419 (1975); D. B. Cline, invited talk at the Washington APS Meeting, 1975 (unpublished); B. C. Barish, invited talk at the Paris Symposium on Neutrino Physics, 1975 (unpublished).

²M. B. Einhorn and B. W. Lee, Phys. Rev. D (to be published); D. D. Reeder, as quoted by Cline, Ref. 1; B. A. Arbuzov, J. J. Gershtein, V. V. Lapin, and V. N. Folomeshkin, Serpukhov Report No. IFVE-75-25 (unpublished); V. Barger, T. Weiler, and R. J. N. Phillips, Univ. of Wisconsin Report No. COO-881-441, 1975 (unpublished).

³L. N. Chang, E. Derman, and J. N. Ng, Phys. Rev. Lett. **35**, 6 (1975); C. H. Albright, Phys. Rev. D **12**, 1319 (1975).

⁴For a clear discussion and a review of the earlier literature, see R. W. Brown and J. Smith, Phys. Rev. D **3**, 207 (1971); R. W. Brown, R. H. Hobbs, and J. Smith, *ibid.* **4**, 794 (1971).

⁵Such particles would have a leptonic decay branching ratio of nearly unity and hence could not account for a reported hadronic γ distribution anomaly which may

be related to the observed dimuons. See A. Benvenuti *et al.*, Phys. Rev. Lett. **34**, 597 (1975).

observed dimuons. See A. Benvenuti *et al.*, Phys. Rev. Lett. **34**, 597 (1975).

⁶Y. Tanikawa and S. Watanabe, Phys. Rev. **113**, 1344 (1957). For further references see the review by C. H. Llewellyn Smith, Phys. Rep. **3C**, 261 (1972). Our results can be used to calculate charged scalar boson production for any of the scalar boson models discussed in this review.

⁷The observed dimuon cross section is about 1% of the single muon inclusive cross section, which in turn (for incident neutrinos) is approximately 0.75×10^{-38} cm² (E/GeV).

⁸A. K. Mann and T. Y. Ling (private communication).

⁹We are indebted to Professor A. K. Mann for a discussion of this point.

¹⁰This conclusion might be evaded only if the inelastic contribution to the B production cross section is strongly dominant, rather than being, as suggested by the calculations of Ref. 4 in the ordinary vector boson case, an order 50% correction.

¹¹See, for example, G. von Gehlen, Nuovo Cimento **30**, 859 (1963).